

Classical Spin Liquid State in the $S = \frac{5}{2}$ Heisenberg Kagome Antiferromagnet $\text{Li}_9\text{Fe}_3(\text{P}_2\text{O}_7)_3(\text{PO}_4)_2$

E. Kermarrec^{1,*}, R. Kumar,¹ G. Bernard,¹ R. Hénaff,¹ P. Mendels,¹ F. Bert,¹
P. L. Paulose,² B. K. Hazra,³ and B. Koteswararao^{4,†}

¹Université Paris-Saclay, CNRS, Laboratoire de Physique des Solides, 91405 Orsay, France

²Department of Condensed Matter Physics and Materials Science, TIFR, Mumbai 400 005, India

³School of Physics, University of Hyderabad, Hyderabad 500046, India

⁴Department of Physics, Indian Institute of Technology Tirupati, Tirupati 517506, India

(Received 4 February 2021; revised 14 July 2021; accepted 16 September 2021; published 6 October 2021)

We investigate the low temperature magnetic properties of a $S = \frac{5}{2}$ Heisenberg kagome antiferromagnet, the layered monodiphosphate $\text{Li}_9\text{Fe}_3(\text{P}_2\text{O}_7)_3(\text{PO}_4)_2$, using magnetization measurements and ^{31}P nuclear magnetic resonance. An antiferromagnetic-type order sets in at $T_N = 1.3$ K and a characteristic magnetization plateau is observed at $1/3$ of the saturation magnetization below $T^* \sim 5$ K. A moderate ^{31}P NMR line broadening reveals the development of anisotropic short-range correlations concomitantly with a gapless spin-lattice relaxation time $T_1 \sim k_B T / \hbar S$, which may point to the presence of a semiclassical nematic spin-liquid state predicted for the Heisenberg kagome antiferromagnetic model or to the persistence of the zero-energy modes of the kagome lattice under large magnetic fields.

DOI: 10.1103/PhysRevLett.127.157202

Magnetic frustration sets as a playground for the discovery of new exotic phases of quantum matter. The Heisenberg antiferromagnetic model on the kagome lattice (KHAF) constitutes the archetype of the frustration in two dimensions, whose ground-state and exotic spin dynamics still remain topical questions in quantum magnetism even after 30 years of research [1–5].

Early on, Chalker *et al.* [6] highlighted the distinctive magnetic properties of the classical ($S = \infty$) KHAF, for which thermal fluctuations select a spin nematic, or coplanar, ground state via the order-by-disorder mechanism in zero field [7,8], with spins on a single triangle oriented at 120° from each other [Fig. 1(e)]. Its spin dynamics is governed by zero-energy soft modes, i.e., special lines of weather vane defects [9]. The order-by-disorder mechanism is also responsible for the remarkable existence of semiclassical fractional plateaus of magnetization in frustrated magnets [1,10–14]. In particular, the $1/3$ plateau—a hallmark of frustration [1,15]—arising from collinear *uud* spin configurations [Fig. 1(d)], has been observed in the triangular compounds Cs_2CuBr_4 [16] and $\text{RbFe}(\text{MoO}_4)_2$ [17–19] but remains debated and/or difficult to observe for quantum kagome antiferromagnets with large interaction [20] or with deviations from the pure KHAF model [21,22].

More recently, the phase diagram of the KHAF in an external field was revisited with state-of-the-art numerical methods, notably tensor network formalism [23,24], density matrix renormalization group [14], or exact diagonalization [13]. It encompasses fully “quantum” phases and semiclassical plateaus, including the $1/3$ plateau that

appears for all values of spin S . The specific aspect of the $1/3$ plateau of the classical kagome lattice under an applied field was pinpointed by finite-temperature Monte Carlo studies which showed that thermal fluctuations favor a classical collinear spin-liquid phase [25,26] at $M = \frac{1}{3} M_{\text{sat}}$, made of a macroscopic number of degenerate *uud* states.

The comparison with classical experimental candidates has remained challenging for long as naturally occurring kagome lattice are rare. The jarosite family $\text{AFe}_3(\text{OH})_6(\text{SO}_4)_2$ (with A^+ typically an univalent cation) is held up as a paragon of the classical KHAF [1,27,28]. They all (but $\text{A}^+ = \text{D}_3\text{O}^+$ [29]) display long range ordering into a $q = 0$ structure, as a result of a deficient kagome

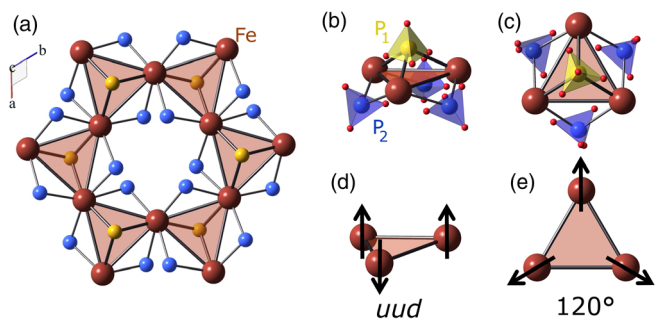


FIG. 1. (a) Schematic structure of LiFePO illustrating the corner-sharing triangular lattice made of Fe^{3+} , $S = \frac{5}{2}$ (brown). Li and O atoms are omitted for clarity. (b),(c) Fe atoms are magnetically coupled through PO_4 chemical groups with two different phosphorus sites: P_1 (yellow) and P_2 (blue). Illustration of the up-up-down *uud* (d) and of the 120° ordered structure (e).

network and/or of perturbative anisotropic terms. Furthermore, their large antiferromagnetic interaction $J \sim 600$ K requires unattainable applied magnetic fields in order to reach the $1/3$ plateau.

In this Letter, we investigate the low temperature magnetic properties of the layered iron monodiphosphate $\text{Li}_9\text{Fe}_3(\text{P}_2\text{O}_7)_3(\text{PO}_4)_2$ (LiFePO), a $S = \frac{5}{2}$ Heisenberg kagome antiferromagnet material with a moderate exchange $J \sim 1$ K. LiFePO thus offers the opportunity to probe and finely explore experimentally the phase diagram of the classical KHAF under applied field. Our measurements reveal a clear $1/3$ magnetization plateau with an extended spin-liquid regime characterized by exotic spin dynamics.

LiFePO belongs to the family of monodiphosphates which were primarily studied for their electronic transport properties in the context of battery materials [30]. LiFePO crystallizes in the centrosymmetric trigonal space group $P\bar{3}c1$ where Fe^{3+} ($S = \frac{5}{2}$) atoms form corner-sharing triangles, topologically equivalent to a regular kagome lattice (Fig. 1), with a strong Heisenberg character ($L \simeq 0$).

The macroscopic magnetic susceptibility is shown as a function of temperature in Fig. 2(a). The susceptibility obeys a Curie-Weiss law, $C/(T - \theta_{\text{CW}})$, with $\theta_{\text{CW}} = -11(2)$ K, corresponding to an antiferromagnetic exchange interaction $J \sim 1$ K [31]. At $T = T_N = 1.3$ K a sharp peak in the magnetic susceptibility signals the onset of an antiferromagnetic order (AFMO) under 1 T [Fig. 2(a)]. The transition temperature T_N is reduced as compared to $|\theta_{\text{CW}}| = 11$ K because of the frustration and the bidimensionality inherent to the kagome geometry. $\text{Li}_9\text{Fe}_3(\text{P}_2\text{O}_7)_3(\text{PO}_4)_2$ thus shows a correlated paramagnetic regime between 1.3 and ~ 10 K. We also note that under a 6 T field the peak amplitude is greatly reduced and T_N slightly increases to 1.8 K, in agreement with NMR (see below), which suggests a nontrivial phase diagram.

Above 10 K, $S = 5/2$ spins are in a paramagnetic regime and $M(B)$ evolves almost linearly from 0 to 16 T. As T is decreased, a pronounced curvature is observed toward the saturated value $M_{\text{sat}} = 5 \mu_B$, as shown in Fig. 2(b). For $T < T^* \simeq 5$ K the slope of the magnetization clearly diminishes before increasing again, in the vicinity of $\sim M_{\text{sat}}/3$. Figure 2(c) shows the derivative dM/dH which firmly confirms the existence of a narrow $1/3$ magnetization plateau developing below T^* . The evolution of the $1/3$ plateau is quantified by the size of the dip, $\Delta(dM/dH)$, and is shown as a function of T in Fig. 2(d). It displays a smooth crossover from a paramagnet for $T > T^*$ to the plateau phase, i.e., a classical collinear spin-liquid phase formed by the set of the uud states that remain degenerate at $M = M_{\text{sat}}/3$, with no clear sign of symmetry breaking like for a gas-liquid-type transition. In the $T \ll |\theta_{\text{CW}}|$ limit, its width can be estimated theoretically from Ref. [25] to ~ 1.5 T in agreement with our experimental value of ~ 1.6 T (FWHM).

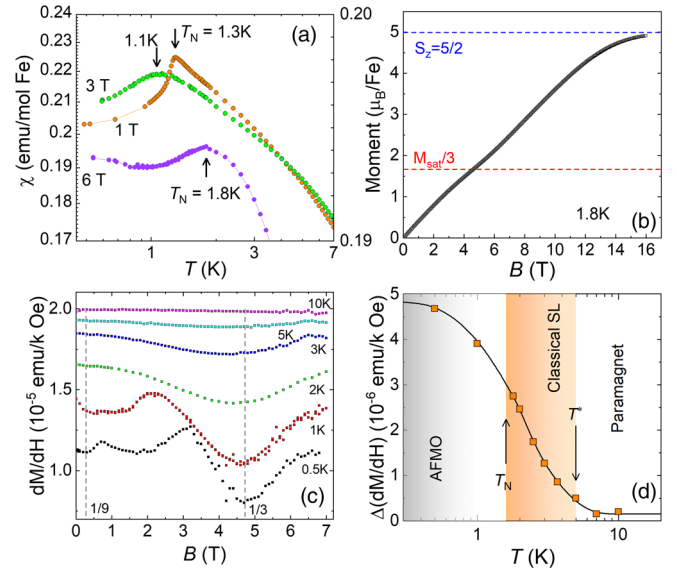


FIG. 2. (a) Magnetic susceptibility χ measured under 1 T, 3 T (left axis), and 6 T (right axis) showing antiferromagnetic transitions at T_N . (b) M vs B measured at $T = 1.8$ K shows a saturated value $M_{\text{sat}} \sim 5 \mu_B/\text{Fe}$ and a $1/3$ plateau for $B \sim 4.75$ T. (c) Derivative dM/dH as a function of temperature (with a constant offset for clarity). The dip at ~ 5 T signals the onset of the $1/3$ plateau for $T = T^*$. (d) Evolution of the dip of the derivative of the magnetization, $\Delta(dM/dH)$, with temperature (orange squares). Line is a guide to the eye. The classical spin-liquid phase emerges below $T^* \simeq 5$ K, followed by an antiferromagnetic order (AFMO) below T_N .

The most recent theoretical phase diagram under applied fields has been computed using numerical tensor network methods. It shows three different incompressible phases or magnetization plateaus besides the $1/3$ plateau [24]. The $1/9$ plateau is only expected for the most quantum case ($S = \frac{1}{2}$). The others (one-magnon and two-magnon plateaus [24]) should appear for all values of S and lie very close to the saturation, respectively, at $43/45$ and $41/45$ for $S = \frac{5}{2}$. These plateaus remain absent in our 1.8 K data but a clear conclusion is difficult and would require applying magnetic fields higher than 16 T. The absence of the C_6 rotational symmetry of our $S = \frac{5}{2}$ Fe^{3+} lattice may also be detrimental to these semiclassical phases.

In order to gain more insights into the magnetic properties of LiFePO, we performed ^{31}P NMR measurements. $\text{Li}_9\text{Fe}_3(\text{P}_2\text{O}_7)_3(\text{PO}_4)_2$ naturally contains two very sensitive NMR nuclei: ^{31}P ($I = 1/2$, $\gamma/2\pi = 17.23467$ MHz/T) and ^7Li ($I = 3/2$, $\gamma/2\pi = 16.54607$ MHz/T). The NMR spectra were obtained with $\nu_0 = \gamma B_0/2\pi = 109.732$ MHz for the ^{31}P local probe with $I = 1/2$, avoiding any quadrupolar effects on the NMR resonance line, using the standard $\pi/2 - \tau - \pi$ pulse sequence, with $\tau = 20 \mu\text{s}$.

Figure 3 displays the evolution of the ^{31}P NMR spectrum with temperature. Two NMR lines, accounting for the two ^{31}P sites (labeled as 1 and 2) expected from the

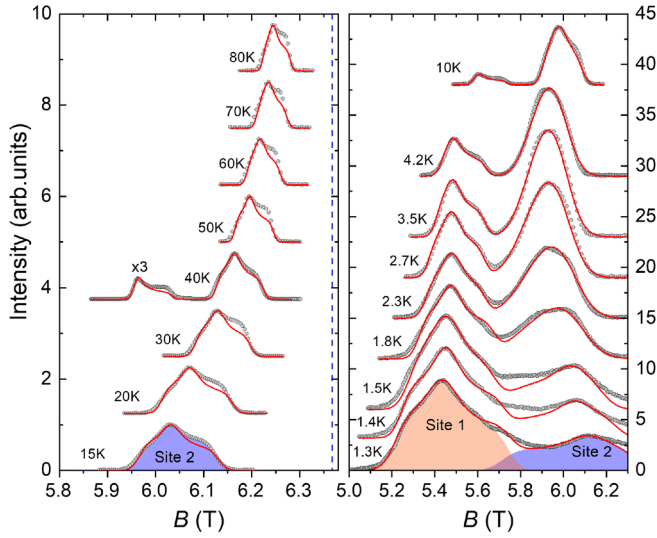


FIG. 3. Temperature dependence of the ^{31}P NMR spectra (circles) measured as a function of applied magnetic field B for LiFePO_4 , from 80 to 1.3 K. The phosphorus located on site (1) is only observed at low T [magnified at 40 K ($\times 3$)], due to strong T_2 relaxation effects. The red line is a fit to Eq. (1) (see text) from which the tensor components K are extracted. Vertical dashed line indicates the reference field $B_0 = 6.3669$ T.

structure [30] [Figs. 1(a) and 1(b)], are clearly visible below 10 K. The NMR intensity relative to site (1) gradually decreases as the temperature is increased, and finally escapes our NMR time window above 50 K, due to a fast relaxation, i.e., a shortening of the T_2 transverse relaxation time ($T_2 < 5\text{--}10 \mu\text{s}$). The ^{31}P NMR Knight shift $\mathbf{K} = A_{\text{hf}}\chi / (g\mu_B\hbar\gamma)$ provides a direct measurement of the local magnetic susceptibility tensor χ . Following the common convention [32] in spherical coordinates, the eigenvalues of \mathbf{K} relate to the shift of the NMR line $\Delta B = B_0 - B$ in the applied field B through [33]:

$$\frac{\Delta B}{B} = K_{\text{iso}} + K_{\text{ax}}(3\cos^2\theta - 1) + K_{\text{ani}}\sin^2\theta \cos 2\phi. \quad (1)$$

The spectra for sites (1) and (2) could be well fitted using Eq. (1) for an isotropic powder distribution (Fig. 3). The mismatch between observed (circles) and simulated (red line) intensities is due to an anisotropic T_2 spin-spin relaxation time, as confirmed by measurements using different duration τ between the pulses (not shown). While site (1) and site (2) probe the same magnetic Fe^{3+} ions, the anisotropic components of the Knight shift tensor are best revealed from site (2) and we thus focus on that NMR line in the following [31]. We then extract the temperature dependence of the components of the Knight shift tensor for site (2), as shown in Fig. 4.

In the paramagnetic regime (300–10 K), the NMR line shape of site (2) is anisotropic and shows a pronounced shoulder on its right-hand side. However, above 10 K,

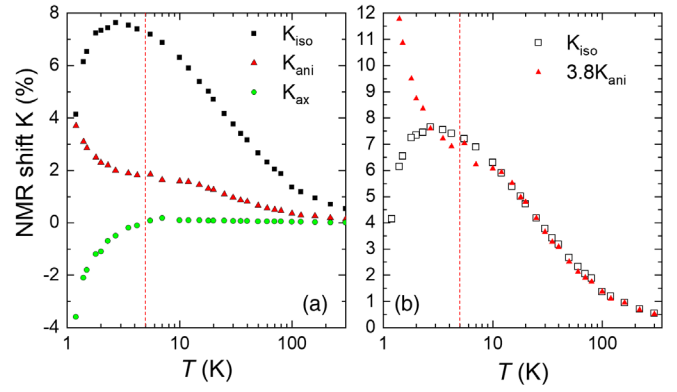


FIG. 4. (a) Components of the NMR shift \mathbf{K} as a function of temperature for site 2. (b) In the paramagnetic regime, K_{iso} and K_{ani} scale with each other showing that the magnetic susceptibility is isotropic above T^* . The red vertical dashed line indicates T^* .

K_{iso} and K_{ani} are found to scale with each other (Fig. 4) and thus the spectrum could be well fitted using a unique T -dependent parameter—an isotropic magnetic susceptibility $\chi(T)$ —with $K_{\text{iso}} = A_{\text{hf}}^{\text{iso}}\chi(T)$, $K_{\text{ani}} = A_{\text{hf}}^{\text{ani}}\chi(T)$, and $K_{\text{ax}} \approx 0$. The T -independent components of the hyperfine tensor per Fe atom are $A_{\text{hf}}^{\text{iso}} = 2.21(3)$ kOe/ μ_B and $A_{\text{hf}}^{\text{ani}} = 0.591(5)$ kOe/ μ_B for site (2). An anisotropic hyperfine coupling tensor is a usual feature of ^{31}P NMR.

Upon cooling below $T^* = 5$ K the NMR line shape evolves and reveals the development of a strongly temperature-dependent anisotropy, which can thus only be ascribed to the magnetic susceptibility. The decrease of K_{iso} signals the development of antiferromagnetic correlations when $T < |\theta_{\text{CW}}| = 11$ K, and clearly indicates the onset of a correlated magnetic phase. Both site (1) and site (2) reveal an anisotropic susceptibility as K_{ani} and K_{ax} undergo an abrupt change, a remarkable feature for Heisenberg spins. The correlated magnetic phase observed for $B \sim 6$ T and $1.3 < T < 10$ K, for which $M \sim \frac{1}{3}M_{\text{sat}}$, seems thus consistent with the theoretically expected, strongly anisotropic, collinear phase.

We now use ^{31}P NMR to investigate the magnetic fluctuations on and around this 1/3-plateau phase. The spin-lattice relaxation rate $1/T_1$ probes the imaginary part of the dynamic susceptibility $\chi''_{\perp}(\nu, q)$ at low energy ($\nu \sim 100$ MHz) through

$$\frac{1}{T_1} = \frac{\gamma^2}{g^2\mu_B^2} k_B T \sum_q |A_{\text{hf}}(q)|^2 \frac{\chi''_{\perp}(\nu, q)}{2\pi\nu} \quad (2)$$

and was determined through the saturation recovery method, with a $\pi/2 - \Delta t - \pi/2 - \tau - \pi$ pulse sequence, from 1.3 to 300 K, at the maximal intensity of site (2) (Fig. 5) for three different applied fields (6.37, 4.75, and 2.375 T) [31]. Four different regimes in temperature can be identified. A peak is clearly observed for $T \sim 1.5$ K,

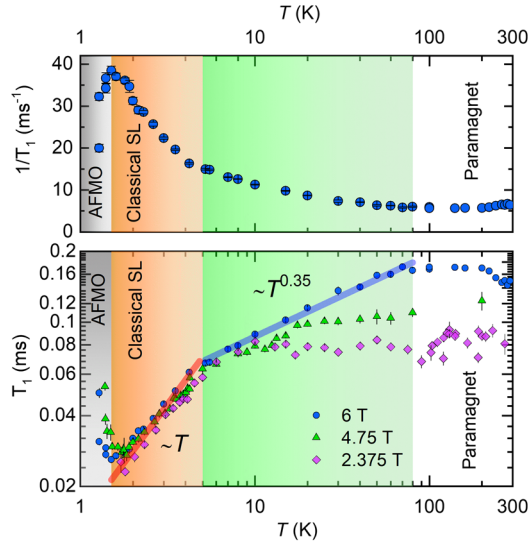


FIG. 5. $1/T_1$ (up) and T_1 (bottom) probed by ^{31}P NMR as a function of temperature in LiFePO. Four different regimes can be identified: a static antiferromagnetic-type order (AFMO, gray), a classical spin-liquid phase (orange), an atypical high- T regime (green), and high- T paramagnetic phase. The classical spin-liquid phase displays spin dynamics with a linear law $T_1 = \beta T$ (red line, see text).

close to the transition temperature T_N , which separates the static magnetic order from a classical spin-liquid state for $T_N < T < T^*$ for which $T_1 \sim T$ (thick red line in Fig. 5). An estimate of the real exponent is difficult for such narrow regime, notably because of critical fluctuations expected just above T_N . A crossover is observed at $T = T^* \sim 5$ K, and the dynamics is now dominated by a higher spin-lattice relaxation rate for $T^* < T < 80$ K, with an atypical power law behavior $\alpha = 0.35(3)$ (blue line) observed for $B = 6.37$ T, which persists well above $|\theta_{\text{CW}}|$, up to ~ 80 K. For this regime, the relaxation is clearly impacted by the applied field, and we speculate that lattice vibrational modes [34] are responsible for the unusual behavior observed here. Finally, T_1 levels off in the high- T paramagnetic regime. The Moriya paramagnetic limit gives the T -independent rate $1/T_1^\infty = \gamma^2 g^2 A_{\text{hf}}^2 S(S+1) / 3z_1 \sqrt{2\pi\nu_e}$ [35,36] in magnetic insulators, where $\nu_e = J\sqrt{2zS(S+1)}/3/h$ the exchange frequency, with $z_1 = 2$ the number of probed Fe and $z = 4$ the number of magnetic nearest neighbors of a Fe atom. Using $A_{\text{hf}} = A_{\text{hf}}^{\text{iso}}$ and the experimental value $T_1^\infty = 0.05(3)$ ms extrapolated at $B \rightarrow 0$ [31], the formula leads to $J = 0.7(3)$ K, in reasonable agreement with $J \sim 1$ K. We note that lithium diffusion likely starts to contribute to the relaxation above 250 K.

We now discuss more specifically the classical spin-liquid phase observed in the T range 1.5–5 K in the context of theoretical predictions. The low- T dynamics of the classical Heisenberg kagome antiferromagnet has been investigated early on by Monte Carlo simulations

[6,37,38]. They gave evidence for the role of thermal fluctuations in selecting a coplanar short-range order via the order-by-disorder mechanism for $T \rightarrow 0$. Short-range nematic spin correlations are predicted to survive at low T with nondispersive soft-magnon modes [39], a characteristic feature associated with the large degeneracy inherent to the kagome lattice. Numerical simulations of the spin autocorrelation function yield $\langle S(0)S(t) \rangle \sim e^{-\nu t}$ for $H = 0$ [1,38,40,41], with $\nu = ck_B T / \hbar S$ ($c \sim 1$) [1,42]. The kagome bilayer compound $\text{SrCr}_8\text{Ga}_4\text{O}_{19}$ was the first experimental candidate to hint at such spin dynamics, yet with an important contribution from quantum fluctuations [38,43–45] and spin vacancies [46]. Later on, inelastic neutron scattering exposed a T -linear inverse relaxation rate in deuterium jarosite over the extended temperature range $0.06 < T/J_{\text{cl}} < 1$ [29], with $J_{\text{cl}} = JS(S+1)$. Here, the T dependence of $1/T_1$ can be inferred from ν through the Redfield formula:

$$\frac{1}{T_1} = \frac{2\gamma^2 \Delta^2 \nu}{\nu^2 + \gamma^2 B^2} \simeq \frac{2\gamma^2 \Delta^2}{\nu}, \quad (3)$$

where Δ is the amplitude of the fluctuating field at the phosphorus position. Using the constant high- T value T_1^∞ , this leads to $T_1 = \beta T$ with $\beta = ck_B T_1^\infty / \nu_e \hbar S$. In LiFePO, the dynamical behavior of T_1 could be well fitted to such a law, with no adjustable parameter but $c = 1.2(1)$ (thick red line in Fig. 5), giving firm evidence of the spin-liquid phase within the T range $0.2 < T/J_{\text{cl}} < 0.6$ with $J_{\text{cl}} = 8.25$ K.

In a more recent work [41], Taillefer *et al.* characterized the dynamics for the long time scales appropriate for NMR using semiclassical numerical techniques, and predicted two different low temperature regimes in the $B \rightarrow 0$ limit: (i) a cooperative, classical, spin-liquid regime with $T_1 \sim T$ in line with what is discussed above and (ii) a coplanar dynamical regime for $T/J_{\text{cl}} < 0.005$ with a strong anisotropic relaxation dominated by weather vane defects modes. Since $J_{\text{cl}} = 8.25$ K, our measurements down to 1.3 K in LiFePO give only access to the region $T/J_{\text{cl}} > 0.2$, i.e., the high- T paramagnetic and cooperative spin-liquid phases, before residual interactions apparently lift the degeneracy and produce the antiferromagnetic transition. The observed thermal behavior of our spin-lattice relaxation rate, $T_1 \sim T$, seems to show that this dynamics unexpectedly persists under moderate applied fields ($B \leq 6$ T). This can perhaps be understood because similar zero-energy excitations exist within the uud manifold of the $1/3$ plateau. Furthermore, the short-range anisotropic correlations that develop above T_N according to our NMR local susceptibility measurements may indicate either that the nematic correlations are still present for $T_N < T < T^*$, or that we lie close to a quasistatic magnetic order. In the light of our results, a theoretical study of the spin dynamics under applied fields, in and around the $1/3$ -phase, would be

highly relevant to confirm the origin of the dynamics observed in NMR.

In conclusion, we have identified a new classical $S = \frac{5}{2}$ Heisenberg kagome antiferromagnet that displays the $1/3$ magnetization plateau predicted a long time ago. Our ^{31}P NMR measurements further identified a classical spin-liquid regime for $T_N < T < T^*$, for which the time scale of the spin dynamics is set by the temperature only, with $T_1 \sim T$, in very good agreement with numerical estimates. Additional experimental and theoretical work would be needed to single out the true signatures of the nematic spin liquid of the $1/3$ plateau from the spin fluctuations inherent to the kagome lattice, and how the latter evolve under large applied magnetic fields. The discovery of archetypal magnetic frustration relevant to the kagome lattice in LiFePO offers great perspectives to improve our knowledge of classical and quantum fluctuation effects in zero and applied fields in the KHAF. In LiFePO, further elastic and inelastic neutron scattering studies could help revisiting the central question of the selection of the $q = 0$ or $q = \sqrt{3} \times \sqrt{3}$ ground state in such model and also confirming the relevance of a simple, nearest-neighbor exchange Hamiltonian. LiFePO and other members of this family [Cr^{3+} ($S = \frac{3}{2}$), V^{3+} ($S = 1$)] will certainly open new avenues to search for quantum phases relevant to the KHAF.

It is a pleasure to acknowledge useful discussion with Professor S. Greenbaum on lithium diffusion, P. Berthet and C. Decorse for sharing their expertise on samples synthesis of lithium oxides, and M. Zhitomirsky on the theory of classical kagome antiferromagnets. E. K. and R. S. acknowledge financial support from the labex PALM for the QuantumPyroMan project (ANR-10-LABX-0039-PALM). B. K. R. thanks for the support from the DST Inspire faculty fund and thanks S. Srinath (UoH) for allowing the sample preparation. This work was supported by the French Agence Nationale de la Recherche under Grant No. ANR-18-CE30-0022-04.

*Corresponding author.

edwin.kermarrec@universite-paris-saclay.fr

†Corresponding author.

koteswararao@iittp.ac.in

- [1] *Introduction to Frustrated Magnetism*, edited by C. Lacroix, P. Mendels, and F. Mila (Springer, Berlin, 2011).
- [2] M. R. Norman, *Rev. Mod. Phys.* **88**, 041002 (2016).
- [3] C. Broholm, R. J. Cava, S. A. Kivelson, D. G. Nocera, M. R. Norman, and T. Senthil, *Science* **367**, eaay0668 (2020).
- [4] P. Khuntia, M. Velazquez, Q. Barthélemy, F. Bert, E. Kermarrec, A. Legros, B. Bernu, L. Messio, A. Zorko, and P. Mendels, *Nat. Phys.* **16**, 469 (2020).
- [5] J. Wang, W. Yuan, P. M. Singer, R. W. Smaha, W. He, J. Wen, Y. S. Lee, and T. Imai, *Nat. Phys.* (2021), <https://doi.org/10.1038/s41567-021-01310-3>.
- [6] J. T. Chalker, P. C. W. Holdsworth, and E. F. Shender, *Phys. Rev. Lett.* **68**, 855 (1992).
- [7] J. Villain, R. Bidaux, J.-P. Carton, and R. Conte, *J. Phys. (Paris)* **41**, 1263 (1980).
- [8] C. L. Henley, *Phys. Rev. Lett.* **62**, 2056 (1989).
- [9] I. Ritchey, P. Chandra, and P. Coleman, *Phys. Rev. B* **47**, 15342(R) (1993).
- [10] A. Honecker, J. Schulenburg, and J. Richter, *J. Phys. Condens. Matter* **16**, S749 (2004).
- [11] H. Kageyama, K. Yoshimura, R. Stern, N. V. Mushnikov, K. Onizuka, M. Kato, K. Kosuge, C. P. Slichter, T. Goto, and Y. Ueda, *Phys. Rev. Lett.* **82**, 3168 (1999).
- [12] Y. H. Matsuda, N. Abe, S. Takeyama, H. Kageyama, P. Corboz, A. Honecker, S. R. Manmana, G. R. Foltin, K. P. Schmidt, and F. Mila, *Phys. Rev. Lett.* **111**, 137204 (2013).
- [13] S. Capponi, O. Derzhko, A. Honecker, A. M. Läuchli, and J. Richter, *Phys. Rev. B* **88**, 144416 (2013).
- [14] S. Nishimoto, N. Shibata, and C. Hotta, *Nat. Commun.* **4**, 2287 (2013).
- [15] D. C. Cabra, M. D. Grynberg, P. C. W. Holdsworth, and P. Pujol, *Phys. Rev. B* **65**, 094418 (2002).
- [16] T. Ono, H. Tanaka, H. Aruga Katori, F. Ishikawa, H. Mitamura, and T. Goto, *Phys. Rev. B* **67**, 104431 (2003).
- [17] T. Inami, Y. Ajiro, and T. Goto, *J. Phys. Soc. Jpn.* **65**, 2374 (1996).
- [18] L. E. Svistov, A. I. Smirnov, L. A. Prozorova, O. A. Petrenko, L. N. Demianets, and A. Ya. Shapiro, *Phys. Rev. B* **67**, 094434 (2003).
- [19] L. E. Svistov, A. I. Smirnov, L. A. Prozorova, O. A. Petrenko, A. Micheler, N. Büttgen, A. Ya. Shapiro, and L. N. Demianets, *Phys. Rev. B* **74**, 024412 (2006).
- [20] R. Okuma, D. Nakamura, and S. Takeyama, *Phys. Rev. B* **102**, 104429 (2020).
- [21] Y. Okamoto, M. Tokunaga, H. Yoshida, A. Matsuo, K. Kindo, and Z. Hiroi, *Phys. Rev. B* **83**, 180407(R) (2011).
- [22] H. Ishikawa, M. Yoshida, K. Nawa, M. Jeong, S. Krämer, M. Horvatić, C. Berthier, M. Takigawa, M. Okami, A. Miyake, M. Tokunaga, K. Kindo, J. Yamaura, Y. Okamoto, and Z. Hiroi, *Phys. Rev. Lett.* **114**, 227202 (2015).
- [23] T. Picot and D. Poilblanc, *Phys. Rev. B* **91**, 064415 (2015).
- [24] T. Picot, M. Ziegler, R. Orús, and D. Poilblanc, *Phys. Rev. B* **93**, 060407(R) (2016).
- [25] M. E. Zhitomirsky, *Phys. Rev. Lett.* **88**, 057204 (2002).
- [26] M. V. Gvozdikova, P.-E. Melchy, and M. E. Zhitomirsky, *J. Phys. Condens. Matter* **23**, 164209 (2011).
- [27] J. E. Greedan, *J. Mater. Chem.* **11**, 37 (2001).
- [28] A. S. Wills, A. Harrison, C. Ritter, and R. I. Smith, *Phys. Rev. B* **61**, 6156 (2000).
- [29] B. Fåk, F. C. Coomer, A. Harrison, D. Visser, and M. E. Zhitomirsky, *Europhys. Lett.* **81**, 17006 (2008).
- [30] S. Poisson, F. d'Yvoire, N. Nguyen-Huy-Dung, E. Bretey, and P. Berthet, *J. Solid State Chem.* **138**, 32 (1998).
- [31] See Supplemental Material at <http://link.aps.org/supplemental/10.1103/PhysRevLett.127.157202> for details on analysis of magnetization and NMR data.
- [32] If (x, y, z) is the vector basis in which the Knight shift tensor \mathbf{K} is diagonal, then the components used here are defined as $K_{\text{iso}} = \frac{1}{3}(K_{xx} + K_{yy} + K_{zz})$, $K_{\text{ax}} = \frac{1}{6}(2K_{zz} - K_{xx} - K_{yy})$, and $K_{\text{ani}} = \frac{1}{2}(K_{yy} - K_{xx})$.

- [33] C. P. Slichter, *Principles of Magnetic Resonance* (Springer, New York, 1996).
- [34] A. J. Vega, P. A. Beckmann, S. Bai, and C. Dybowski, *Phys. Rev. B* **74**, 214420 (2006).
- [35] T. Moriya, *Prog. Theor. Phys.* **16**, 23 (1956).
- [36] E. Kermarrec, A. Zorko, F. Bert, R. H. Colman, B. Koteswararao, F. Bouquet, P. Bonville, A. Hillier, A. Amato, J. van Tol, A. Ozarowski, A. S. Wills, and P. Mendels, *Phys. Rev. B* **90**, 205103 (2014).
- [37] J. N. Reimers and A. J. Berlinsky, *Phys. Rev. B* **48**, 9539 (1993).
- [38] A. Keren, *Phys. Rev. Lett.* **72**, 3254 (1994).
- [39] A. B. Harris, C. Kallin, and A. J. Berlinsky, *Phys. Rev. B* **45**, 2899 (1992).
- [40] J. Robert, B. Canals, V. Simonet, and R. Ballou, *Phys. Rev. Lett.* **101**, 117207 (2008).
- [41] M. Taillefumier, J. Robert, C. L. Henley, R. Moessner, and B. Canals, *Phys. Rev. B* **90**, 064419 (2014).
- [42] R. Moessner and J. T. Chalker, *Phys. Rev. B* **58**, 12049 (1998).
- [43] Y. J. Uemura, A. Keren, K. Kojima, L. P. Le, G. M. Luke, W. D. Wu, Y. Ajiro, T. Asano, Y. Kuriyama, M. Mekata, H. Kikuchi, and K. Kakurai, *Phys. Rev. Lett.* **73**, 3306 (1994).
- [44] D. Bono, P. Mendels, G. Collin, N. Blanchard, F. Bert, A. Amato, C. Baines, and A. D. Hillier, *Phys. Rev. Lett.* **93**, 187201 (2004).
- [45] S.-H. Lee, C. Broholm, G. Aeppli, T. G. Perring, B. Hessen, and A. Taylor, *Phys. Rev. Lett.* **76**, 4424 (1996).
- [46] L. Limot, P. Mendels, G. Collin, C. Mondelli, B. Ouladdiaf, H. Mutka, N. Blanchard, and M. Mekata, *Phys. Rev. B* **65**, 144447 (2002).